Food Chemistry 351 (2021) 129287

Contents lists available at ScienceDirect

Food Chemistry

journal homepage: www.elsevier.com/locate/foodchem

Broadband acoustic resonance dissolution spectroscopy as a rapid tool for the compositional analysis of food powders: A case study of edible salts

Pedram Shoa [a,b,*], Seyed Ahmad Mireei [a], Abbas Hemmat [a], Sara W. Erasmus [c], Saskia M. Van Ruth [b,c,*]

[a] Department of Biosystems Engineering, College of Agriculture, Isfahan University of Technology, Isfahan 84156-83111, Iran
[b] Wageningen Food Safety Research, Wageningen University and Research, P.O. Box 230, 6700 AE Wageningen, the Netherlands
[c] Food Quality and Design Group, Wageningen University and Research, P.O. Box 17, 6700 AA Wageningen, the Netherlands

ARTICLE INFO

Keywords:
Acoustics
BARDS
Composition
Food powder
Morphology
Quantitative analysis

ABSTRACT

Broadband acoustic resonance dissolution spectroscopy (BARDS) is a novel method that can be used for the analysis of food-based powders, which are mainly characterized by their composition and particle morphology. This study aimed to evaluate BARDS for the compositional analysis of food powders. The changes in the BARDS spectra due to the changes in composition and particle morphology of fifteen salt mixtures (constituting of NaCl, KCl, and $MgCl_2$) in five particle size ranges were comprehensively studied. Moreover, different regression methods were utilized to estimate each mixture component content. The results revealed that the average time–frequency spectra of each mixture in a certain particle size class were highly distinct and allowed discrimination from others. The unique spectra of each salt mixture originated from the specific dissolution rate and degassing effect of each constitutive compound. Finally, the accurate prediction of each mixture component content confirmed the consistency and efficiency of the method.

Chemical compounds studied in this article: Magnesium chloride (PubChem CID: 5360315); Potassium chloride (PubChem CID: 4873); Sodium chloride (PubChem CID: 5234).

1. Introduction

Recently, the application of acoustics in food analysis is becoming pervasive due to the advantages of low experimental costs and marginal sample preparation. Acoustic detection methods are product specific. Detection of cracks in eggshells (Sun, Bi, Lin, Zhao, & Cai, 2013), evaluation of fruit firmness, crispness and crunchiness (Tunick et al., 2013), detection of mycotoxins in wheat grains (Juodeikiene et al., 2014), investigation of the rehydration behavior of milk protein (Wu et al., 2019), and the authentication of salts (van Ruth et al., 2019) are all studies in which the acoustic waves have been served to analyze food materials.

Broadband acoustic resonance dissolution spectroscopy (BARDS) is a novel method, developed for the characterization of powders. Its feasibility for the authentication and quality control of food powders has been recently reported in a few papers (van Ruth et al., 2019a; Vos et al., 2016; Wu et al., 2019). In this spectroscopic method, the acoustic spectrum of a powdered substance is generated during the addition and subsequent dissolution of the powder in a solvent (mostly water) by the changes in the frequency of sound, traveling through the dissolution media. The frequency change is due to the emergence, growth, and subsequent elimination of minute air bubbles. The curve related to this frequency-time course is the acoustic spectrum and called the fundamental curve (FC) (Fitzpatrick et al., 2013). Compositional and morphological differences in powders provide curves with various shapes due to the changing physicochemical characteristics of the powder, which can directly or indirectly influence the dissolution process (Fitzpatrick et al., 2012a).

A well discriminative power of the method has been reported between different compounds and even polymorphs with the same composition (Fitzpatrick et al., 2012a). The FC of blends has also been observed as the intermediate curve of two pure ingredients (Fitzpatrick

* Corresponding authors at: Department of Biosystems Engineering, College of Agriculture, Isfahan University of Technology, Isfahan 84156-83111, Iran and Wageningen Food Safety Research, Wageningen University and Research, P.O. Box 230, 6700 AE, Wageningen, the Netherlands.
E-mail addresses: pedram.shoa@ag.iut.ac.ir (P. Shoa), samireei@iut.ac.ir (S.A. Mireei), ahemmat@iut.ac.ir (A. Hemmat), sara.erasmus@wur.nl (S.W. Erasmus), saskia.vanruth@wur.nl (S.M. Van Ruth).

https://doi.org/10.1016/j.foodchem.2021.129287
Received 22 July 2020; Received in revised form 26 December 2020; Accepted 1 February 2021
Available online 15 February 2021

et al., 2012a). However, the need to investigate the behavior of mixtures has been highlighted in other reports (Fitzpatrick et al., 2013, 2012). It was reported that the FC of milk protein concentrate samples with different protein contents was highly discriminable, in which the differences were observed both in the frequential and temporal features of the FC (Vos et al., 2016). The results of a study on sands from coasts in the Netherlands also indicated that both composition and particle morphology play an important role in the shape of the FC (van Ruth, Hettinga, Dekker, & Fitzpatrick, 2019).

Table salt is one of the simplest 'food' powders, which is officially characterized by its sodium chloride (NaCl) content. Natural, often specialty, table salts are unrefined edible salts that recently became popular due to their particular taste and claimed health benefits (Galvis-Sánchez, Lopes, Delgadillo, & Rangel, 2013). In addition to NaCl, these salts are mainly composed of potassium chloride (KCl) and magnesium chloride ($MgCl_2$), which exists in rock and sea salts, respectively. The salt particles may be pure crystals of the main salts (NaCl, KCl, and $MgCl_2$) or the attachment of different salt crystals (Davidson & Slabaugh, 2003). The quality of natural salts is mainly determined by the portion of each of these main components in the final product (Galvis-Sánchez et al., 2013). In the previous study on salt characterization in which BARDS technology was applied, the composition and particle size distributions of natural and reference salts and mixtures thereof, were found to have significant effects on the features of the FC (van Ruth et al., 2019a). A significant correlation was observed between the temporal features of the FC, and the composition and particle size index of the ground and intact samples.

To successfully apply the BARDS technology for the compositional analysis of food powders and suitable applications such as quality control, following goals must be achieved. (1) More comprehensive studies are needed to find the specific physicochemical properties of the powders, which are responsible for the changes in the characteristic features of the FC. These properties are not fully covered in previous studies related to food powders. (2) The effect of the particle size on the acoustic spectra should be studied in more details, so that it could be recognized from the effect of the composition. (3) To evaluate the efficiency of BARDS for the quantitative analysis of food powders, which means to predict the concentration of its main components. The latter was not previously studied. Through the prediction of the composition, one can assure the quality of the product but also detect nonconformities. To achieve these goals in this study, the single, binary, and ternary artificial mixtures of three edible salts (NaCl, KCl, and $MgCl_2$), each in five particle size classes (with a narrow band), were used and regarded as a representative source of a food powder model with changes in the two main attributes of composition and particle morphology.

2. Materials and methods

2.1. Theory of BARDS

The hot chocolate effect (Crawford, 1982) states that the dissolution of a substance in a liquid solvent can reduce the gas solubility of the solution compared to the pure solvent. Therefore, the solution will get oversaturated by those amounts of gas, which have been dissolved in the solvent. The gas oversaturated liquid is not stable; thus, the extra dissolved gases will be absorbed by existing bubbles in the solution. These bubbles can be produced by those amounts of air, entrained to the solvent with solute particles or be nucleated in highly oversaturated solution. The air could be entrained to the solvent with particle collision to liquid surface at the time of the solute introduction. Some amounts of air which are stuck between or adhered to solute particles will also entrain to the solvent at this time. Also, air gaps may present within solute particles which will be released later during the dissolution and produce microbubbles. The air bubbles originated from these three sources are called entrained bubbles.

The presence of air bubbles in a liquid media can impressively reduce the compressibility and insignificantly lessen the density of that media. Thus, based on Newton-Laplace equation (Eq. (1)), the sound velocity in liquid media will be reduced by the presence of air bubbles (Crawford, 1990):

$$v = \sqrt{\frac{1}{k\rho\rho}} \tag{1}$$

where v is the sound velocity in the media with a mass density of ρ and compressibility of k (Douhéret, Davis, Reis, & Blandamer, 2001). Since a resonating dissolution vessel can act as a closed-end sound tube, the wavelength of the sound is constant and equal to one-quarter of the vessel length. The wavelength of the sound is equal to its velocity divided by its frequency; hence the sound velocity is proportional to its frequency at a constant wavelength. According to these facts, Crawford proposed Eq. (2):

$$\frac{v}{u_w} = \frac{freq}{freq_w} = \sqrt{1 + \left(1.49 \times 10^4 (f_a)\right)} \tag{2}$$

where f_a is the volume fraction of bubbles in the liquid, υ_w and $freq_w$ are the velocity and frequency of sound in water with no bubbles, while υ and $freq$ are those of the bubble-filled water (Crawford, 1982; Del Grosso & Mader, 1972). Thus, it is possible to track the bubble volume with the measurement of the sound frequency during the dissolution process. Among the many emerged resonance frequencies with high power, the FC is the one with the lowest variable frequency-time course which relates to the solvent.

The FC has important critical points in time to consider. The first time point after the powder introduction is called the entrain response point (ERP). The F_{ERP} is mostly depended to the volume of entrained bubbles emerge right after the solute introduction to the solvent. Increasing particle size also increases the amount of air entrained with solute introduction. Hence, it is reported that the ERP is mostly related to the particle size rather than the composition of the solute (Fitzpatrick et al., 2014). The overall minimum frequency (F_{min}) is a significant point at which a balance appears between the bubble growth/generation and bubble liberation from the surface of the liquid. This point also indicates the highest bubble volume in the solution. The time (Δt) taken to reach the F_{min} is also an important feature, since it relates to the dissolution rate of the compound. Both F_{min} and Δt are related to the powder's composition as well as its particle size distribution. To analyze the FC, each curve can be assumed as an acoustic spectrum in which each data point is an independent variable. Since the number of those variables is large, it is shown that multivariate analysis methods such as principal components analysis (PCA) can reduce the size of the variable space, and the new obtained space is able to cover most of the variation in the dataset. This space can also provide good discrimination power between sample classes (van Ruth et al., 2019b).

2.2. Materials

Analytical grade salts of NaCl (Merck, 1.06404), KCl (Merck, 1.04936), and $MgCl_2$ (Merck, 1.05833) (VWR International B.V., Amsterdam, the Netherlands) were ground using a commercial coffee grinder (Tristar KM-2270 Tristar, Smartwares Group, Tilburg, the Netherlands). The salts were subsequently passed through different sieves to obtain five different particle size classes with the following codes and the corresponding particle size ranges in parenthesis: E (63–150 μm), D (150–250 μm), C (250–350 μm), B (350–500 μm), and A (500–650 μm). Due to the highly hygroscopic nature of $MgCl_2$ all samples were oven-dried at 103 °C before analysis. The chemical characteristics of the reference salts and their effects on the solution are shown in Table S1 (Supplementary material). Fifteen different salt mixtures for each particle size class were prepared using a simplex lattice mixture design (Gorman & Hinman, 1962), where each one was a mixture of

different portions of the three salts. The pure salts were considered, but also 0, 0.25, 0.50, and 0.75 fractions (w/w) of the three salts in various variations. The composition of the 15 samples is detailed in Table S2, provided as Supplementary material.

2.3. Instrumentation

A broadband acoustic resonance dissolution spectrometer (BARDS Acoustic Science Labs, Cork, Ireland) was utilized to monitor the frequency change of acoustic resonances in the solution during the dissolution of each salt mixture in demineralized water. This spectrometer has a dissolution vessel made of borosilicate, which is suitable for 25 mL solvent (Supplementary material, Fig. S1). A uni-directional, cardio design, condenser microphone (Sony ECM-CS10) with a frequency range of 100 Hz to 16 kHz was used to record the acoustic analog waves. The sound was generated by tapping the vessel wall with a magnetic stirrer at a rotational speed of 300 rpm. The acoustic wave was digitized using a sound card having a 44.1 kHz sampling rate and being able to reconstruct acoustic waves up to 22.1 kHz frequencies according to the sampling theorem, which can cover the microphone sensitivity range (Nyquist, 1928). To obtain the spectrogram, a short-term Fourier transform (STFT) was applied to the digital signal using a fast Fourier transform (FFT) with 16,384 window size.

2.4. Experimental procedure

For each measurement, 0.8 g of solute was dissolved in 25 mL of demineralized water (van Ruth et al., 2019a). Experiments were conducted in a conditioned laboratory with a stable room temperature of 22 ℃ and an atmospheric pressure of ~1 atm, without any heating or cooling of the solvent. Prior to any measurements, gas saturation in the solvent was stabilized through vigorous agitation by shaking the solvent bottle for 60 s and then allowing it to rest for more than 30 min.

During the first 30 s of the measurements, acoustic waves were recorded to measure the resonance frequency of the solvent and the vessel at a steady state. At the 30 s time-point, the solute was automatically added to the solvent using a sample cap which was controlled by an electrical motor. To assure that the curve reaches the same frequency of the first 30 s after the liberation of the bubbles, the signal was recorded for 300 s. The spectra were acquired for each sample mixture. All samples were analyzed in triplicate, and the average spectra over the three replicate measurements per sample mixture were calculated and utilized as the representative of that sample.

2.5. Particle size measurements

A laser diffraction analyzer (Mastersizer 3000, Malvern Instruments, Malvern, UK) alongside an Aero S dry powder dispersion accessory was utilized to measure the particle size distribution of the salt powders. The measurements are based on the theory of diffraction by Fraunhofer, which states that the intensity of scattered light by a particle is directly proportional to the particle size (Li, Li, Bodycomb, & Patience, 2019). Particles disperse and travel through the detection cell by means of airflow with the settings of 2 bar pressure, 3 mm of hoper gap, and a feed rate of 20% using a vibrational feeder. For modeling, particle type was selected as a non-spherical particle with the Fraunhofer approximation. Measurements were recorded once the obscuration was between 0.5 and 6.0 percent. Similar to the previous study, the particle size characteristics were recorded as Dx (50), the median diameter (van Ruth et al., 2019a). The average of triplicate measurements was served in further analysis.

2.6. Data analysis

2.6.1. Spectral analysis

For further analysis, 50 pre-defined time–frequency data points were derived manually from each FC and saved in an Excel file. The bubble volume and its derivative as the bubble volume rate were calculated using Eq. (2) and the Savitsky-Golay transformation of the bubble volume spectra (Savitzky & Golay, 1964). The frequency of ERP (F_{ERP}), the F_{min}, and the Δt of each FC was used as three main curve features and their correlations with the measured particle size Dx(50) were examined using Pearson correlation coefficients (r).

2.6.2. Multivariate analysis

Principal component analysis (PCA) was performed on FC, bubble volume and bubble volume rate spectra. The score plots were demonstrated to explore the discrimination between fifteen salt mixtures, as well as five particle size classes. The loading of each time point variable was also calculated and demonstrated.

Nine different data sets, including the three types of FC, bubble volume, and bubble volume rate spectra, each at three different durations of 90 s, 180 s, and 300 s were created. D(50) was also added to each data set as a variable of particle size in the model. Samples were arranged along the first dimension and variables along the second dimension of the X matrix. Multivariate regression methods were utilized for the prediction of the percentage of each main salt in the mixtures. Since the spectral variables were collinear, and the number of independent variables was high (variable matrix was not full rank), traditional regression models were not suitable. Thus, principal component regression (PCR) and partial least square regression (PLSR) as two linear approaches and support vector regression (SVR) with a Gaussian kernel of radial basis function (RBF) as a non-linear one were utilized.

PCR is a multiple standard regression in which the regressors are principal components (PCs) with the highest eigenvalues, extracted from the PCA of the independent variables matrix X. This method can deal well with collinearity and large number of independent variables, since it maps the variable space into the space of a few orthogonal PCs. The obtained PCs can explain the majority of data variation by using the singular value decomposition (SVD) method (Keithley, Mark Wightman, & Heien, 2009).

PLSR is also a linear regression in which the regressors are latent variables (LV). LVs are orthogonal directions extracted from independent variable space in such a way that they simultaneously correlate with dependent variables. This method is also useful in the case of multicollinearity problem in the independent variable set (Wold, Sjöström, & Eriksson, 2001).

SVR considers a margin of tolerance (ε) tube around the regression hyperplane that those data points placed outside of this margin tube will just be penalized. It reduces the dependency of the model on the training data set. Gaussian RBF was utilized in this study to map the independent variables into a feature space with a higher dimension so that a linear hyperplane can predict the dependent variables (percentage of each salt in the mixture). This strategy makes the regression non-linear and also increased the prediction accuracy since the method is not sensitive to dimensionality (Awad, Khanna, Awad, & Khanna, 2015). In this study, two optimal parameters of the SVR model, C and V, were determined using a heuristic grid search (among different values of 0.1, 1, 10, and 100) for the best validation result.

Two-thirds of the samples were served for training and validating the regression models and one third for the testing. For every three regression models, 10-fold cross-validation was served. Prior to the regression analysis, independent variables (X) were mean-centered and scaled according to their standard deviation. The adjusted coefficient of determination for the prediction (R^2_p) and the root mean square error of the prediction (RMSEP) were calculated as two figures of merit. All data transformation and analysis were carried out using "The Unscrambler X10.4" statistical software package (CAMOAS, Trondheim, Norway). A significance level of 5% ($P < 0.05$) was considered throughout the study.

3. Results and discussion

3.1. Overview of the BARDS spectra

Fig. 1 illustrates a raw spectrogram obtained from a pure NaCl (m1) sample with a particle size class C. After setting the magnetic stirrer into motion at 0 s, several lines with high power emerged as resonance frequencies of different parts of the system, which were evident during the first 30 s of the spectrogram (Fig. 1). After 30 s, the solute was introduced into the solvent, and one of those lines dropped to the F_{ERP} at 33 s due to the emerging bubbles (next data point after 30 s was at 33 s, considered as ERP). There is a 3 s time interval between the solute entrance and the ERP. Therefore, it could be considered that the existing bubbles at the ERP were produced by both the entrained air and also extra dissolved gases in the oversaturated liquid. The entrained bubbles or new generated bubbles can absorb the extra dissolved gases from gas oversaturated solution which is provided by the early dissolved molecules of the solute. As the solute particles were dissolving, bubble volume was increasing by the growth of entrained bubbles or the generation of new bubbles; and reached its maximum at the point of (Δt , F_{min}). These bubbles were liberated from the solution surface after a time, which relates to the size of the bubble and the viscosity of the solution. It was evident that at the end of the FC, where all bubbles were liberated from the media, the resonance frequency restored to the values observed in the first 30 s. This frequency line is called the volume line since the resonance frequency of non-bubbly media changes only by the volume of the water in the vessel (i.e. by changing the length of the acoustic tube and consequently the wavelength of the induced sound). The volume line in the case of this study was observed at ~ 9.0 kHz.

3.2. Spectral interpretation

3.2.1. Single salt mixtures

The average FC, bubble volume, and the bubble volume rate spectra for each salt mixture (m1-m15) are shown in Figs. 2–4 for the particle size class B, respectively. The spectra related to three reference salts are indicated as m1: pure NaCl, m5: pure KCl, and m15: pure $MgCl_2$. Each reference salt had its particular spectrum, completely discriminable from the others. After a sudden depletion in frequency from volume line to the ERP, m1 and m15 exhibited a U-type FC, whereas m5 showed a V-type FC (Fig. 2a, b). For the bubble volume curves, after the appearance of a 0.001 mL, 0.0052 mL, and 0.021 mL volume of bubbles at ERP for m1, m5, and m15 respectively, the bubble volume of m1 and m15, increased to reach their maximum value of 0.0018 mL and 0.036 mL at the time point of 79.4 s and 38.2 s, while for m5, bubble volume decrease logarithmically toward the zero (Fig. 3b). For three reference salts, the shape of the FC and the bubble volume curves were similar as the findings of the previous study (van Ruth et al., 2019a).

The bubble volume rate in Fig. 4, can be considered as the bubble growth/generation rate minus the rate of bubble liberation in the solution, which has not been studied in the previous publications. For the bubble volume rate curves, after a sudden high positive rate of bubble volume at the ERP which is mostly due to the comparison of zero bubble volume at 30 s and the high amount of entrained bubbles appeared at 33 s, m1 started to dissolve slowly with a nearly zero rate of bubble volume; followed by an increase to a local maximum rate. It could be inferred that the gas oversaturation is at its highest value at the time point of the local maximum bubble volume rate, which coincided with the first deflection point on the bubble volume curve (Fig. 3a). The bubble volume rate of m1 then decreased and passed through the zero value at the time point of (Δt, F_{min}), at which the bubble growth/generation and liberation rates had the same values. This decrease continued to reach the minimum negative value, the point that the solution is expected to have its highest bubble liberation rate and appeared as the second deflection point on the bubble volume curve (Fig. 3a). The bubble volume rate then increased to reach the zero value by the end of the bubble liberation process. For m5, a higher positive rate of bubble volume (compared to m1), appears at the ERP, is due to the comparison of zero bubble volume at 30 s and the entrained plus early generated/grown bubbles at 33 s. At the next time point (34.6 s), the bubble volume rate of m5 decreased to its minimum negative value, followed by a gradual increase to the zero value by the end of the bubble liberation. When compared to m1 and m15, the negative values for the bubble volume rate after the ERP (for m5), are due to a lower gas oversaturation provided by the salt powder. Hence, the rate of bubble growth/generation is lower than that of bubble liberation leading to a V-type FC for m5. For m15 (Fig. 4b), after its high positive rate at ERP (higher than that of m1 and m5), bubble volume rate gradually decreased to reach the zero at the time point of F_{min} (m1 and m5 had a sudden reduction after the ERP respectively to about zero and a negative value). This reduction continued to reach the minimum value of bubble volume rate (negative) at which the bubble elimination rate is expected to have its maximum value and coincided by a deflection in the bubble volume curve (Fig. 3b). The rate then increased to the zero value again at the end of the bubble elimination process. These results showed that m1 (NaCl), m5 (KCl), and m15 ($MgCl_2$) had bubble volume rate curves with sinusoidal (with two extremes), logarithmic (with decreasing negative values), and a highly damping exponential shape, respectively. Therefore, the shape of the bubble volume rate curve also seems to be indicative of a powder fingerprint, even more than the FC and bubble volume curves. It is

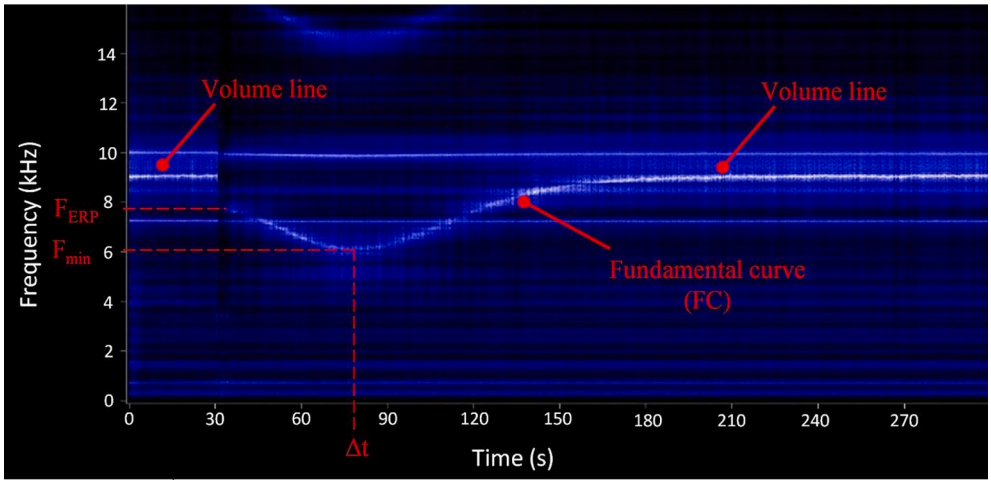

Fig. 1. A broadband acoustic resonance dissolution 726 spectrogram of the m1 (100% NaCl) in particle size class C (250–350 μm). The color intensity refers to the power of the signal.

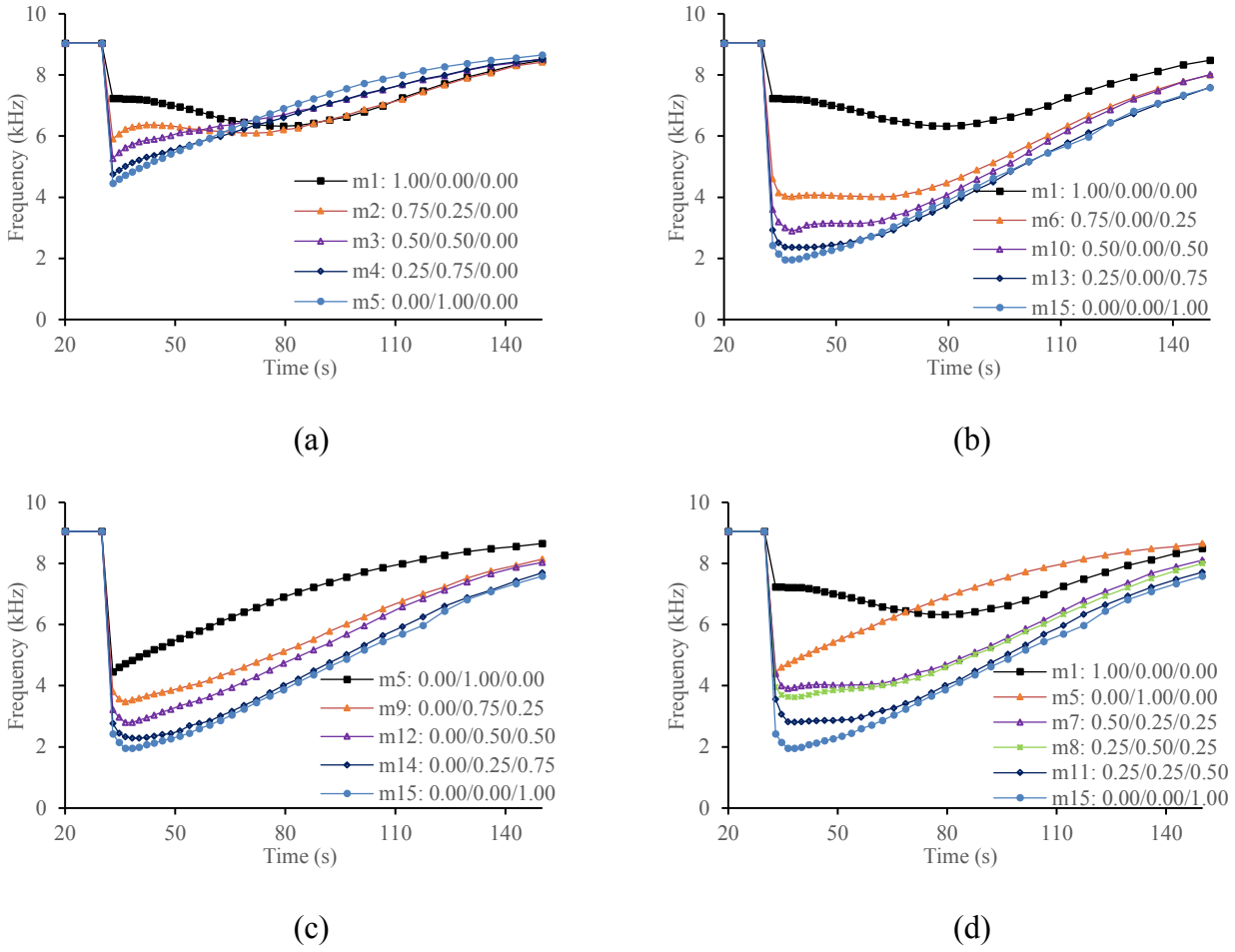

Fig. 2. The fundamental curve averaged from three measurements 729 of single and binary mixtures from (a) NaCl and KCl, (b) NaCl and MgCl2 and (c) KCl and MgCl2; (d) single and ternary mixtures of NaCl, KCl and MgCl2 (particle size class B: 350–500 μm). In the legends, the composition of each mixture is explained by the portions of each salt as mx: NaCl/KCl/MgCl2.

evident that the compound-specific shape of the curve, is a function of the changes in bubble volume rate, which can be considered as the difference between bubble growth/generation and liberation rate (FC shape is not a function of the total bubbles volume that exist in the solution).

The gas solubility reduction could be the main reason for the shape difference of the spectra between KCl and the other two salts. When a solid is dissolved in a liquid, the solubility of gases decreases due to the salting-out effect. This decrease varies with the type of solute (Schumpe, 1993). Furthermore, gas solubility is a function of solution temperature. Based on the ion–dipole interaction between the ions and the water molecules, solution temperature can be changed according to the dissolution enthalpy which is compound-specific (Haynes, Lide, & Bruno, 2016). In this study, according to the dissolution enthalpy and the heat capacity of the salt solutions, the solution temperature is expected to increase by about 12.6 ℃ for m15, and decrease by 1.4 ℃ for m5, and 0.5 ℃ for the m1, after dissolving the samples in the water (Supplementary material, Table S1). Increasing the temperature of the solution can: (1) increase the dissolution rate (Haynes et al., 2016); (2) reduce the gas solubility of the solution by approximately 10% for each 5.0 ℃ increment (Garde, García, Pratt, & Hummer, 1999); and (3) decrease the viscosity of the solution(Haynes et al., 2016; Siepmann & Siepmann, 2013). To show the effect of temperature on the acoustic spectra, pure NaCl (due to its lower dissolution rate) was dissolved in water with six different temperatures (Supplementary material, Fig. S3). As the initial solvent temperature increased, the maximum bubble volume also increased (F_{min} decreased) due to the reduction of gas solubility. The time required to reach this maximum (Δt) was decreased due to the increasing dissolution rate (Fig. S3 a, b). With increasing initial solvent temperature, maximum bubble volume rate has been increased due to the higher gas oversaturation and hence higher bubble growth/generation rate (Fig. S3 c). The minimum bubble volume rate (in negative value) was decreased by increasing initial solvent temperature, which is due to the decreasing solution viscosity. These results are in line with previous studies on sodium carbonate, where a reduction in Δt was reported due to temperature increment, and against the result of having no changes in F_{min} due to the temperature effect (Fitzpatrick et al., 2012a).

Considering the dissolution enthalpy and the salting out effect, the gas solubility is expected to reduce by ~ 14.5% for m1(NaCl), ~7.5% for m5 (KCl), and 40.7% for m15 ($MgCl_2$) after dissolving the samples in water (Supplementary material, Table S1). A lower gas solubility reduction of KCl resulted in a lower level of gas oversaturation and hence, a lower rate of bubble growth/generation. It should also be noted that m5 has a higher dissolution rate than m1 (Supplementary material, Table S1). The other scenario is that a large portion of m5 sample was dissolved in early seconds after introducing the solute to the solvent (30–33 s), since the dissolution rate of KCl is significantly higher than that of NaCl (Supplementary material, Table S1). Hence, a considerable portion of gas oversaturation was provided early before the liberation of those bubbles entrained with solute particles. Entrained bubbles can grow by absorbing the gas oversaturation and increase the bubble volume in a more rapid way than generating new bubbles. This phenomena can result in a greater bubble volume and its rate for m5 before ERP (33

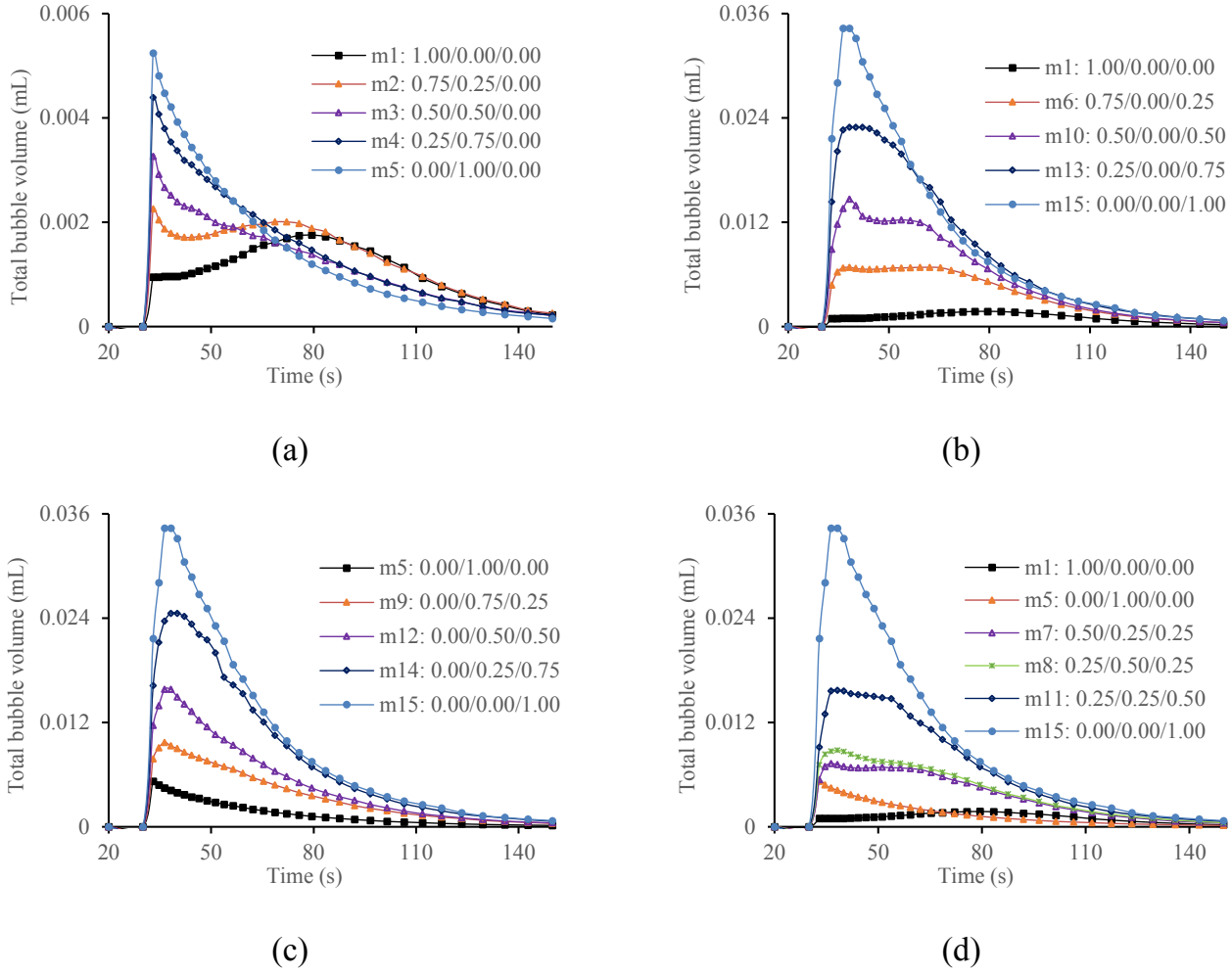

Fig. 3. The bubble volume averaged from three measurements 734 of single and binary mixtures from (a) NaCl and KCl, (b) NaCl and MgCl2 and (c) KCl and MgCl2; (d) single and ternary mixtures of NaCl, KCl and MgCl2 (particle size class B: 350–500 μm). In the legends, the composition of each mixture is explained by the portions of each salt as mx: NaCl/KCl/MgCl2.

s) compared to m1 (Fig. 3a, 4a), and negative bubble volume rates for the time points after ERP, making a V-typed FC. Due to the high gas solubility reduction, and the very high dissolution rate of the $MgCl_2$ (highly hygroscopic nature and increased solution temperature), m15 had the lowest F_{ERP}, highest bubble volume and highest bubble volume rate at the ERP compared to m1 and m5. At each particle size class, m1 had the highest F_{ERP}, lowest bubble volume and lowest bubble volume rate at ERP which is mainly due to its low dissolution rate.

Comparing m1 and m15 at the equilibrium time point of zero bubble volume rate (F_{min}), higher maximum bubble volume, and lower F_{min} of m15 is mainly due to the higher gas solubility reduction of m15. Lower Δt for m15 than for m1, can be the consequence of the higher dissolution rate of $MgCl_2$. Dissolution rate is an important factor, which can be impressed by both the composition and morphology of a powder (Siepmann & Siepmann, 2013). It can affect the timing and the value of F_{min}. It is expected to have a minimum frequency time point, being later with lower in bubble volume for the samples with lower dissolution rates. This behavior is because a significant amount of entrained bubbles will be liberated from the surface before the solution reaches its F_{min} time point. Hence, its maximum bubble volume would be reduced. With an increase in dissolution rate, the solution reaches its highest concentration of solute in a shorter time, and consequently its maximum gas oversaturation and bubble volume time points occur in shorter durations.

The minimum bubble volume rate, which is a negative value, can be dedicated by those physicochemical characteristics of the solution related to the bubble elimination rate. The minimum bubble volume rate is -0.00018 mLs^{-1} for m1, -0.00038 mLs^{-1} for m5, and -0.0022 mLs^{-1} for m15. The viscosity of the solution is responsible for the bubble elimination rate, which can be different from that of the pure solvent. The solution viscosity is solute-specific (Phang & Stokes, 1980; Zhang & Han, 1996). In addition, the viscosity of the solution is a function of the temperature (Haynes et al., 2016). Dynamic viscosity of the solution is expected to be ~ 5.6% and ~ 2.2% higher than the initial solvent after the dissolution of m1 and m5. But it remains almost constant after the dissolution of m15 at the molarity used in this study (Supplementary material, Table S1). At higher viscosity, the bubble liberation rate decreases due to the lower terminal velocity of the bubbles in the solution and vice versa (Snabre & Magnifotcham, 1998). This means that the bubble liberation rate could be reduced after dissolving m1 and m5 while it may remain constant after the addition of m15.

Furthermore, the surface tension of water increases by dissolving electrolytes due to electrostatic forces or solute–solvent attraction. This increment is solute-specific (Dutcher, Wexler, & Clegg, 2010). Moreover, the surface tension of water and brines reduces by temperature increment (Vargaftik, Volkov, & Voljak, 1983). The surface tension of the solution is expected to increase by ~ 1.3%, ~1.1%, and ~ 0% for m1, m5, and m15 accordingly after the dissolution of the samples. Increasing surface tension of the liquid can decrease the size of bubbles due to higher pressure difference or gas oversaturation needed to grow a

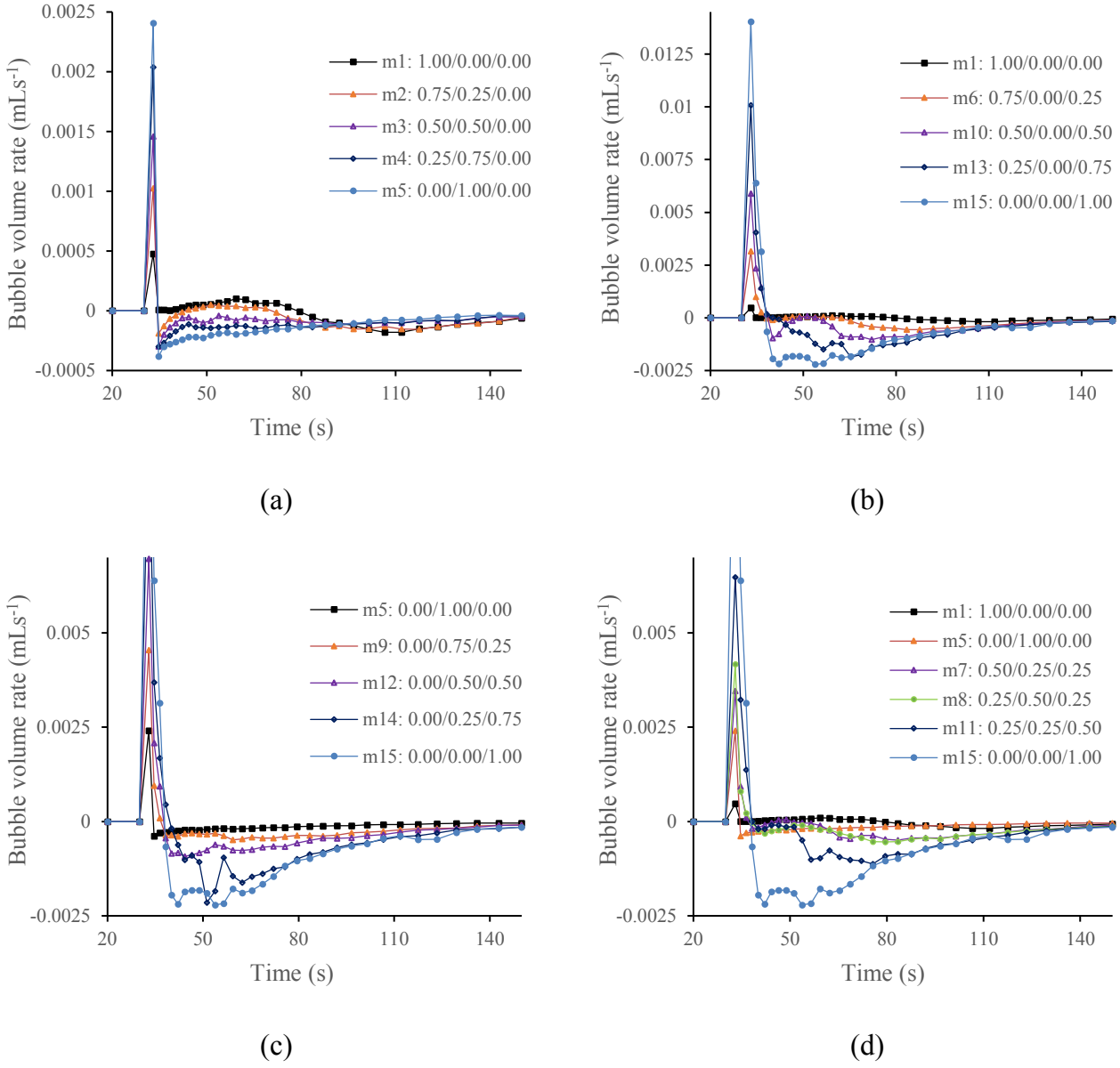

Fig. 4. The bubble volume rate averaged from three measurements 739 of single and binary mixtures from (a) NaCl and KCl, (b) NaCl and MgCl2 and (c) KCl and MgCl2; (d) single and ternary mixtures of NaCl, KCl and MgCl2 (particle size class B: 350–500 μm). In the legends, the composition of each mixture is explained by the portions of each salt as mx: NaCl/KCl/MgCl2.

bubble (Zahedi, Saleh, Moreno-Atanasio, & Yousefi, 2014). Meanwhile, bigger bubbles have higher terminal velocity, hence a higher bubble liberation rate is expected for the solutions with lower surface tension. Thus, as the dynamic viscosity and the surface tension of the solution decreases from m1 to m5 and then m15, the minimum bubble volume rate of these solutions reduces, and the bubble elimination rate increases.

3.2.2. *Binary salt mixtures*

Fig. 2a, Fig. 3a, and Fig. 4a are the FC, bubble volume and bubble volume rate spectra, related to salt mixtures with the gradual transition from 100% NaCl to 100% KCl. The frequency and bubble volume at ERP, decreased and increased respectively with the increasing percentage of KCl. This trend was also reported in the previous study with different mixtures and particle size ranges (van Ruth et al., 2019a). Salt mixtures containing a higher NaCl content (m1, m2 and m3) had two deflection points on their FC, while for the mixture with a lower NaCl content (m4), the deflection points were almost vanished. The fingerprint of NaCl on the FC and bubble volume curves can be seen as two deflection points. However, the first one seems to be more related to the presence of NaCl in the mixture. Furthermore, for those mixtures containing KCl, the bubble volume rate curves started with an increasing negative value at an early stage of the dissolution. This sign can be considered as a feature related to the presence of KCl. Since the dissolution rate of NaCl is lower than that of KCl (Supplementary material, Table S1), the fingerprint of KCl appears at the first part of the curves, while the later parts of the curve are more related to the presence of NaCl.

The FC, bubble volume, and bubble volume rate curves of the binary mixture transition from 100% NaCl to 100% $MgCl_2$ are shown in Fig. 2b, Fig. 3b, and Fig. 4b, respectively. The F_{ERP} decreased, and the bubble volume at ERP increased by the increasing portion of $MgCl_2$ which is due to the high dissolution rate and high gas solubility reduction of $MgCl_2$. Same trends has been observed in the previous study which can confirm the current findings (van Ruth et al., 2019a). The global minimum point on the FC appeared around the 38 s time-point of the experiment for all salt mixtures containing $MgCl_2$, which can also be seen as a point on the

bubble volume rate curve passing through the zero value (Fig. 4b). The maximum bubble volume, which appears on the global minimum point of the FC, increased with the increasing percentage of $MgCl_2$. A local minimum around 42 s is obvious on the bubble volume rate curve, which appears as the second deflection point on the FC. Furthermore, a decreasing positive slope at early time-points, after the introduction of the solute into the solvent, can be seen for the salt mixtures containing $MgCl_2$. Appearing the maximum bubble volume at around 38 s, a decreasing positive bubble volume rate after ERP, and the lowest bubble volume rate around 42 s, can be used as the most robust fingerprint features of the $MgCl_2$ salt. As shown on the bubble volume rate curve of pure NaCl (m1) (Fig. 4b), the two extreme points as two deflection points on the FC can be clearly seen for the salt mixtures containing high concentrations of NaCl (i.e. m6 and m10). The appearance of the fingerprints related to the NaCl after the ones related to the $MgCl_2$ is due to the lower dissolution rate of NaCl. The local minimum bubble volume rate around 42 s decreased with the increasing percentage of $MgCl_2$. It means that the bubble liberation rate increases with the increase in percentage of $MgCl_2$. This fact is due to the ability of growing the bigger bubbles with the higher terminal velocity in the brine of $MgCl_2$, compared to the brines of NaCl and KCl (as already discussed in section 3.2.1).

The FC, bubble volume, and bubble volume rate curves related to the salt mixtures, changing from 100% KCl (m5) into 100% $MgCl_2$ (m15) are shown in Fig. 2c, Fig. 3c and Fig. 4c. Again, a decreasing positive slope followed by a minimum frequency around 38 s on the FC (Fig. 2c), and a minimum bubble volume rate around 42 s (Fig. 4c) appeared for the salt mixtures containing $MgCl_2$. By increasing the contribution of $MgCl_2$ in the salt mixtures, F_{ERP} and F_{min} were reduced without showing any signs of the KCl fingerprint. This fact can be due to the very high dissolution rate and degassing effect of $MgCl_2$, which overruled the emergence of the KCl fingerprints at the beginning of the FC and bubble volume rate curves.

3.2.3. Ternary salt mixtures

The FC, bubble volume, and bubble volume rate curves related to three ternary salt mixtures are shown in Fig. 2d, Fig. 3d and Fig. 4d. A substantial reducing effect on the F_{ERP} and F_{min}, due to the increasing $MgCl_2$ percentage is noticeable which is in line with the results of the ternary mixtures, studied in the previous study (van Ruth et al., 2019a). Again, a positive decreasing bubble volume rate after the ERP, a maximum bubble volume around 38 s, and the minimum bubble volume rate around 42 s are apparent for m7, m8, and m11, which were previously recognized as the fingerprint of $MgCl_2$ on the binary salt mixtures (section 3.2.2). After a minimum, around 42 s, two other extreme points on the bubble volume rate curve are obvious and could be the same points observed previously for the salt mixtures containing NaCl (recognized as its fingerprint). As it was observed for the binary salt mixtures containing $MgCl_2$ and KCl, no fingerprint was detected for the KCl salt.

According to the findings mentioned above, it is evident that each component of a mixture had its signature(s) on the FC, bubble volume, and/or bubble volume rate curves. The ordering of the appearance of these signatures was dictated by the order of dissolution rates of the components. The higher the dissolution rate, the earlier the fingerprint appeared on the spectra. In same particle size distribution, the value of the spectra at featured time points can be related to the percentage of each component in a mixture. This process is somehow similar to what happens in chromatography in which each substance fingerprint emerges at a particular retention time with an intensity related to the concentration of that mater. The main goal of the authentication of salts and other food powders is the estimation of the percentage of each component in the sample. Thus, the spectral values at the featured time points, recognized as the fingerprint of a component, could be used as the input for a regression model to predict the portion of that component or to classify the powders with different qualities. Further studies on different kind of food powders are needed to confirm this claim.

3.3. Effect of particle size

Particle size, as a morphological factor, could change the FC in two ways. Firstly, by changing the dissolution rate due to the changes in the interfacial diffusion surface area per amount of solute (Siepmann & Siepmann, 2013). Secondly, by influencing the amount of entrained gas to the solvent (Fitzpatrick et al., 2013). The latter is owing to the changes in the air trapped within or between the particles and also air entrapment at the time of particle collision on the solvent's surface; bigger particles entrap higher volumes of gas (Marston, Vakarelski, & Thoroddsen, 2011; Mosharraf & Nyström, 1995). Thus, finer particles introduce a lower amount of gas at the time of introduction, hence increase the F_{ERP}. On the other hand, higher dissolution rates rapidly oversaturate the solution with gas, producing lower Δt values. For m1, the local maximum bubble volume rate (after ERP) seems to be increased by the decreasing particle size Dx(50), but the correlation was not significant (Supplementary material, Fig. S3a, Fig. S4a, Fig. S5a). This result was expected due to the increasing effect of particle size reduction on the dissolution rate and hence, the bubble growth/generation rate. The minimum bubble volume rate of different particle size classes of m1 samples had no significant correlation with particle size Dx (50). It was expected since the final molarity and hence, the viscosity and surface tension which can affect the bubble liberation from the solution, was the same for all particle size classes. For m15 (Supplementary material, Fig. S3b, Fig. S4b, Fig. S5b), the bubble volume rate was decreased by particle size reduction at time points before the F_{min}. The decreasing bubble volume rate by the particle size reduction may be due to the decrease in entrained bubbles, which acts as the growth centers. Bubble growth can increase the bubble volume more rapidly than the bubble generation. Thus, lower growth centers can decrease the bubble growth/generation rate and hence the total bubble volume rate. Same as m1, there was no significant correlation between the minimum bubble volume rate of different particle size classes of m15 and the particle size Dx(50). For m5 (Supplementary material, Fig. S3c, Fig. S4c, Fig. S5c), the maximum bubble volume rate at ERP decreased significantly by particle size reduction which is due to the comparison between zero and reducing bubble volume at ERP with particle size reduction. A minimum bubble volume rate occurred right after the ERP and decreased (negative value) with the increase in particle size for the m5 samples. It could be due to the lower dissolution rate of bigger particles, which reduced the bubble growth/generation rate at early time-points after introducing the powder to the solvent. As a result, the aggregate bubble volume rate would have a larger negative rate. It can also be due to the higher terminal velocity of bigger bubbles entrained with bigger solute particles which increases the bubble elimination rate.

For those salt mixtures containing a high percentage of KCl or NaCl (m1:m5), there was a sharp, significant negative correlation, existed between F_{ERP} and Dx(50) (Table 1, Supplementary material Fig. S6). It indicates that larger particles can entrain higher amounts of gas at the time of introduction to the solvent, which is in line with the previous studies that reported a shift of the FC to higher frequencies due to a reduction of particle size (Fitzpatrick et al., 2012a; Marston et al., 2011; van Ruth et al., 2019a). For these salt mixtures, the correlation between F_{min} and Dx(50) was also inversely significant (Table 1). Conversely, for the salt mixtures containing high amounts of $MgCl_2$ (m10:m15), the correlation between F_{ERP} and Dx(50) was positively significant but with a moderate slope (Table 1; Supplementary material, Fig. S6). These results may be because of the higher dissolution rate of the salt mixtures containing high amounts of $MgCl_2$, which increases the effect of early dissolved solute molecules on the gas oversaturation and bubble volume at ERP. For most of these salt mixtures (except m12), there was no significant correlation between F_{min} and Dx(50).

A significant negative correlation exists between Δt and Dx(50) for most of the salt mixtures (Table 1). While a positive correlation was

Table 1
The Pearson correlation coefficients (r) between the 753 FC features and particle size parameter Dx(50).

Mixture	FERP *vs* Dx(50)	Fmin *vs* Dx(50)	Δt *vs* Dx(50)
m1	−0.98**	−0.76**	−0.60*
m2	−0.99**	−0.98**	−0.93**
m3	−0.99**	−0.99**	−0.85**
m4	−0.99**	V-type	V-type
m5	−0.98**	V-type	V-type
m6	0.86**	0.85**	−0.84**
m7	0.67**	−0.33n.s.	−0.9**
m8	−0.61*	−0.96**	−0.84**
m9	−0.92**	−0.97**	0.77**
m10	0.96*	0.44n.s.	−0.86**
m11	0.88**	−0.48n.s.	−0.84**
m12	0.74**	−0.83**	0.59*
m13	0.91**	0.45n.s.	−0.43n.s.
m14	0.93**	−0.40n.s.	0.82**
m15	0.94**	−0.17n.s.	0.87**

* and ** stands for significant levels of 0.05 and 0.01, respectively. n.s. refers to non-significant correlations.

expected due to the higher dissolution rate of finer particles, the obtained negative correlation may be related to the way that finer particles interact with the solvent. After the addition of finer particles (classes D and E), they agglomerated and settled on the bottom of the vessel. With this behavior, the interfacial diffusion surface area for dissolution significantly reduced. Hence, the dissolution rate was decreased, and the Δt was increased. Since the agglomeration did not happen uniformly for every measurement, the coefficient of variation of F_{min} (averaged from different mixtures) increased from 1.05% for the particle size class A, to the 2.64% for the class E. For Δt, this coefficient of variation increased from 0.95% for the particle size class A to the 3.15% for the particle size class E. Consequently, it could be stated that, if the goal of these measurements is to find a reproducible fingerprint for powders according to their composition, it is better to avoid the use of samples with very fine particles, due to their tendency to agglomerate.

3.4. Multivariate analysis

3.4.1. PCA results

PCA was performed using the FC, bubble volume, and bubble volume rate spectra for all the salt mixtures, and the results were demonstrated in Fig. 5. Overall, 99% of the variation in the data was explained by the

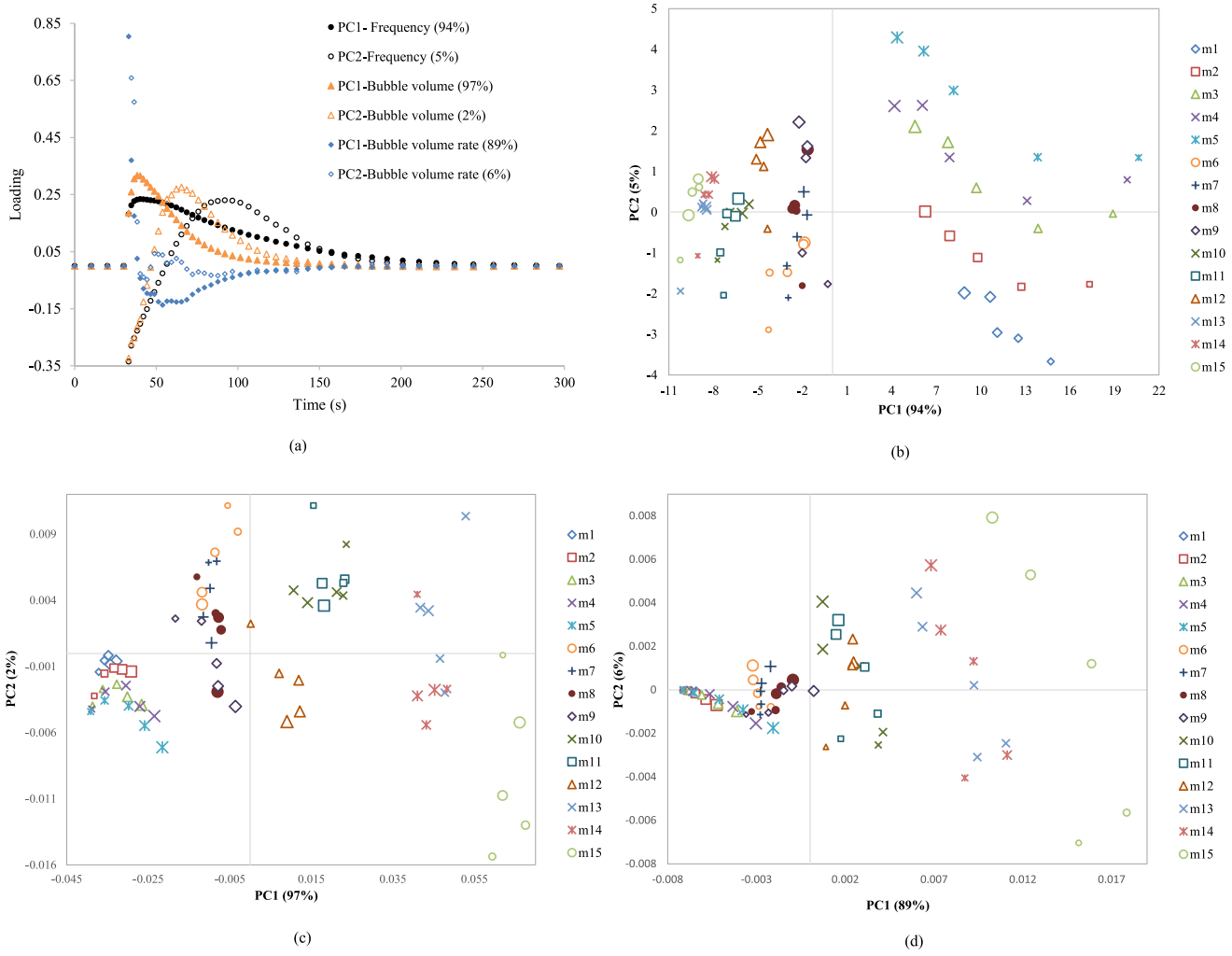

Fig. 5. The principal component analysis (PCA) results: (744 a) loadings of two main PCs for the time point variables of the fundamental curve (FC), bubble volume and bubble volume rate spectra. (b) plot of the two main PC scores of the fifteen salt mixtures, using frequency spectra time points (c) plot of the two main PC scores of the fifteen salt mixtures, using bubble volume spectra time points (d) plot of the two main PC scores of the fifteen salt mixtures, using bubble volume rate spectra time points. Three size of markers indicates A (500–650 μm), B (350–500 μm), C (250–350 μm), D (150–250 μm) and E (150–63 μm) particle size classes. For interpretation of the colors refer to the web version of the paper.

first two principal components (PCs) for the FC and bubble volume spectra, and 95% for the bubble volume rate spectra. The loadings indicate the influence of each time point variable by diverging from the zero value to ± 1 (Fig. 5a). The first 30 s had zero loading values due to the constant volume line. For each variable set, loadings first diverged from the zero, reached its maximum, and then converged back to zero by the end of the experiment. It was evident that the variables, related to the growth/generation phase at early seconds after the introduction of the solute to the solvent, were more important than those related to the elimination phase at the later time-points of the experiment. It was observed that the final part of the FC for a given salt mixture and particle size class was not uniform among different measurements. This was due to the non-uniform amount of the bubbles which adheres to the vessel wall at the end of the measurement. Loading curves of the bubble volume and the bubble volume rate spectra converged to zero at earlier time points (~90 s) comparing to the FC data (~150 s).

According to the score plots derived from FC spectra (Fig. 5b) five mixture classes (m1:m5) with zero percent of $MgCl_2$ were located on the right side of the diagram (positive PC1 values). Whereas, the salt mixtures containing $MgCl_2$ were found at the left side (negative PC1 values). On the right side of the plot, the fourth quadrant (negative PC2) was occupied by those samples having high contributions of the NaCl (100% and 75%) in their mixtures. According to previous studies, most of the mineral natural food-grade salts have NaCl portions in this range. On the left side of the plot, mixtures with zero percentage of NaCl were located in the second quadrant with positive PC2 values. On the left side of the diagram, as the percentage of the $MgCl_2$ increased, the PC1 reduced to higher negative values. The m6, m7, m8, and m9 had almost the same position on the PC1 axis due to their equal portion of 25% $MgCl_2$. While by decreasing the percentage of NaCl from m6 to m9, the PC2 values increased. This trend is also obvious for m10, m11 and m12 with same 50% $MgCl_2$, and for m13 and m14 with 75% of $MgCl_2$, each had almost same positions on the PC1 axis. In these mixtures the decrease of PC2 was due to an increase in the contribution of NaCl.

For the PC score plot derived from the bubble volume and bubble volume rate spectra (Fig. 5c and d), mixtures distributed along PC1 axis due to their percentage of $MgCl_2$, higher PC1, higher contribution of this salt in the mixture. Samples were also distributed along PC2 due to their contribution of NaCl, in which the PC2 increased with the increasing NaCl percentage. For the PCA derived from FC spectra, the distance between different salt mixtures decreased as the contribution of $MgCl_2$ increased; whereas for the PCA derived from the bubble volume and the bubble volume rate spectra, the discrimination between different mixtures seems to be increased by the percentage of $MgCl_2$. A slight change in PC1 seems to be responsible for the changes in KCl percentage for every PCA score plot. As it was observed on the FC and bubble volume rate spectra, the fingerprint of $MgCl_2$ was coincided temporally on the ones for KCl in some of the salt mixtures. Hence, it is also expected for them to distribute on the same principal axis (PC1). It is obvious that different particle size classes of a salt mixture provided a significant variation along PC2 axis. Since the goal of salt authentication is to predict or classify according to the composition of a substance, it is necessary to consider a variable for particle size in the regression or the classification model. According to the PC score plots, it is evident that the data points related to the finest particle size class E, located far from other classes. In most of the cases, it did not follow the trend that exists between the other four courser classes. This evidence is due to the effect of their non-uniform dissolution and it causes a reducing reproducibility of the BARDS method (explained in section 3.3).

3.4.2. Regression results

Table S3, provided in suplimentary materials, shows the test set validation results of each model using three types of spectra and three time durations (length of the spectra). The FC spectra provided the best results (models) for predicting the NaCl and KCl contents, compared to the bubble volume and bubble volume rate spectra at each regression method and length of the spectra. This is while for the prediction of $MgCl_2$ content, the RMSEP of two linear models (PCR and PLSR) decreased from 10% to 3% by using bubble volume and bubble volume rate spectra instead of FC spectra. By using the SVR method, the RMSEP for the prediction of $MgCl_2$ was the same 3% for every type of spectra. Among three different regression methods, SVR provided the highest performance in terms of R^2_p of mixture components using FC spectra ($R^2_p = 0.95$, 0.94, and 0.99 for NaCl, KCl, and $MgCl_2$, respectively). This regression model provided a convincing low RMSEP of 7% for NaCl, 8% for KCl, and 3% for $MgCl_2$ by using the first 90 s of the FC spectra, where the loadings of two main PCs had their highest values. It was observed that each salt mixture had its particular behavior regarding the changes in particle size. Furthermore, the spectral effect of changing the percentage of one component in the salt mixture was depended to the other components presents in the mixture, due to the interactions between different electrolytes in the solution. Hence, it is reasonable to expect better results from a non-linear regression model (SVR with RBF kernel) comparing to linear models (PCA or PLSR).

4. Conclusions

To investigate the potential of BARDS for the compositional analysis of food powders, the acoustic spectra of three reference salts and their mixtures in different particle size classes (as representative food powder models) were measured and analyzed. BARDS was capable of characterizing the composition of different salt mixtures in various particle size ranges. The results of this study revealed that not only the dissolution rate but also the other physicochemical properties of the powders; including dissolution enthalpy or the level of gas solubility reduction, are responsible for the changes observed in the FC, bubble volume and bubble volume rate spectra, among samples with different compositions. Thereby, the technology generates a unique fingerprint for each salt mixture. It was demonstrated that the bubble volume rate spectra; and in some cases, the FC and bubble volume spectra, presented distinct features for salts and their mixtures. PCA showed that the salt's composition and particle sizes interfere and result in a mingled effect on the acoustic signatures, which will complicate compositional predictions. Among different regression methods, SVR led to better predictability of mixture component content, compared to PLSR and PCR. The satisfactory results of the developed SVR model confirmed the consistency and efficiency of the BARDS technique in quantitative analysis of food powders. This study is a step forward in paving the way for the utilization of BARDS for the quality control and/or authentication of powdered foods based on their composition.

Funding

The first author received a fellowship from the Iranian Ministry of Science Research and Technology (MSRT).

CRediT authorship contribution statement

Pedram Shoa: Conceptualization, Methodology, Validation, Formal analysis, Investigation, Data curation, Writing - original draft, Visualization. **Seyed Ahmad Mireei:** Supervision, Data curation, Writing – review & editing, Funding acquisition. **Abbas Hemmat:** Supervision, Writing – review & editing, Funding acquisition. **Sara W. Erasmus:** Methodology, Investigation, Writing – review & editing. **Saskia M. Van Ruth:** Supervision, Conceptualization, Methodology, Resources, Writing – review & editing, Project administration, Funding acquisition.

Declaration of Competing Interest

The authors declare that they have no known competing financial interests or personal relationships that could have appeared to influence the work reported in this paper.

Acknowledgments

The authors gratefully appreciate the technical support from Wageningen Food Safety Research (WFSR) and the financial support from Isfahan University of Technology, Isfahan, Iran. The authors also would like to express their gratitude towards Eric Cuijpers, Erwin Brouwer, and Alex Koot for their valuable help and guidance.

Appendix A. Supplementary data

Supplementary data to this article can be found online at https://doi.org/10.1016/j.foodchem.2021.129287.

References

Awad, M., Khanna, R., Awad, M., & Khanna, R. (2015). Support Vector Regression. In Efficient Learning Machines (pp. 67–80). Apress. 10.1007/978-1-4302-5990-9_4.

Crawford, F. S. (1982). The hot chocolate effect. *American Journal of Physics, 50*(5), 398–404.

Crawford, F. S. (1990). Hot water, fresh beer, and salt. *American Journal of Physics, 58*(11), 1033–1036.

Davidson, C. F., & Slabaugh, M. R. (2003). Salt crystals - Science behind the magic. *Journal of Chemical Education, 80*(2), 155–156. https://doi.org/10.1021/ed080p155.

Del Grosso, V. A., & Mader, C. W. (1972). Speed of Sound in Pure Water. *The Journal of the Acoustical Society of America, 52*(5B), 1442–1446.

Douhéret, G., Davis, M. I., Reis, J. C. R., & Blandamer, M. J. (2001). Isentropic Compressibilities—Experimental Origin and the Quest for their Rigorous Estimation in Thermodynamically Ideal Liquid Mixtures. *ChemPhysChem, 2*(3), 148–161.

Dutcher, C. S., Wexler, A. S., & Clegg, S. L. (2010). Surface Tensions of Inorganic Multicomponent Aqueous Electrolyte Solutions and Melts. *Journal of Physical Chemistry A, 114*(46), 12216–12230.

Fitzpatrick, D., Evans-Hurson, R., Fu, Y., Burke, T., Krüse, J., Vos, B., McSweeney, S. G., Casaubieilh, P., & Keating, J. J. (2014). Rapid profiling of enteric coated drug delivery spheres via Broadband Acoustic Resonance Dissolution Spectroscopy (BARDS). *Analyst, 139*(5), 1000–1006.

Fitzpatrick, D., Evans-Hurson, R., Krüse, J., Vos, B., McSweeney, S., Casaubieilh, P., & O'Gorman, É. (2013). The relationship between dissolution, gas oversaturation and outgassing of solutions determined by Broadband Acoustic Resonance Dissolution Spectroscopy (BARDS). *Analyst, 138*(17), 5005–5010. https://doi.org/10.1039/c3an36838f.

Fitzpatrick, D., Krüse, J., Vos, B., Foley, O., Gleeson, D., O'Gorman, E., & O'Keefe, R. (2012a). Principles and Applications of Broadband Acoustic Resonance Dissolution Spectroscopy (BARDS): A Sound Approach for the Analysis of Compounds. *Analytical Chemistry, 84*(5), 2202–2210.

Fitzpatrick, D., Scanlon, E., Krüse, J., Vos, B., Evans-Hurson, R., Fitzpatrick, E., & McSweeney, S. (2012b). Blend uniformity analysis of pharmaceutical products by Broadband Acoustic Resonance Dissolution Spectroscopy (BARDS). *International Journal of Pharmaceutics, 438*(1-2), 134–139. https://doi.org/10.1016/j.ijpharm.2012.07.073.

Galvis-Sánchez, A. C., Lopes, J. A., Delgadillo, I., & Rangel, A. O. S. S. (2013). Sea salt. *Comprehensive Analytical Chemistry, 60*, 719–740. https://doi.org/10.1016/B978-0-444-59562-1.00026-8.

Garde, S., García, A. E., Pratt, L. R., & Hummer, G. (1999). Temperature dependence of the solubility of non-polar gases in water. *Biophysical Chemistry, 78*(1-2), 21–32. https://doi.org/10.1016/S0301-4622(99)00018-6.

Gorman, J. W., & Hinman, J. E. (1962). Simplex Lattice Designs for Multicomponent Systems. *Technometrics, 4*(4), 463–487. https://doi.org/10.1080/00401706.1962.10490034.

Haynes, W. M., Lide, D. R., & Bruno, T. J. (2016). In *CRC Handbook of Chemistry and Physics*. CRC Handbook of Chemistry and Physics. CRC Press. https://doi.org/10.1201/9781315380476.

Juodeikiene, G., Vidmantiene, D., Basinskiene, L., Cernauskas, D., Klupsaite, D., Bartkiene, E., Petrauskas, A., & de Koe, W. J. (2014). Recent advances in the rapid acoustic screening of deoxynivalenol in wheat grains. *World Mycotoxin Journal, 7*(4), 517–525. https://doi.org/10.3920/WMJ2013.1677.

Keithley, R. B., Mark Wightman, R., & Heien, M. L. (2009). Multivariate concentration determination using principal component regression with residual analysis. *TrAC Trends in Analytical Chemistry, 28*(9), 1127–1136. https://doi.org/10.1016/j.trac.2009.07.002.

Li, H.e., Li, J., Bodycomb, J., & Patience, G. S. (2019). Experimental Methods in Chemical Engineering: Particle Size Distribution by Laser Diffraction—PSD. *Canadian Journal of Chemical Engineering, 97*(7), 1974–1981. https://doi.org/10.1002/cjce.23480.

Marston, J. O., Vakarelski, I. U., & Thoroddsen, S. T. (2011). Bubble entrapment during sphere impact onto quiescent liquid surfaces. *Journal of Fluid Mechanics, 680*, 660–670. https://doi.org/10.1017/jfm.2011.202.

Mosharraf, M., & Nyström, C. (1995). The effect of particle size and shape on the surface specific dissolution rate of microsized practically insoluble drugs. *International Journal of Pharmaceutics, 122*(1-2), 35–47. https://doi.org/10.1016/0378-5173(95)00033-F.

Nyquist, H. (1928). Certain Topics in Telegraph Transmission Theory. *Transactions of the American Institute of Electrical Engineers, 47*(2), 617–644. https://doi.org/10.1109/T-AIEE.1928.5055024.

Phang, S., & Stokes, R. H. (1980). Density, viscosity, conductance, and transference number of concentrated aqueous magnesium chloride at 25°C. *Journal of Solution Chemistry, 9*(7), 497–505. https://doi.org/10.1007/BF00647738.

Savitzky, A., & Golay, M. J. E. (1964). Smoothing and Differentiation of Data by Simplified Least Squares Procedures. *Analytical Chemistry, 36*(8), 1627–1639. https://doi.org/10.1021/ac60214a047.

Schumpe, A. (1993). The estimation of gas solubilities in salt solutions. *Chemical Engineering Science, 48*(1), 153–158. https://doi.org/10.1016/0009-2509(93)80291-W.

Siepmann, J., & Siepmann, F. (2013). Mathematical modeling of drug dissolution. *International Journal of Pharmaceutics, 453*(1), 12–24. https://doi.org/10.1016/j.ijpharm.2013.04.044.

Snabre, P., & Magnifotcham, F. (1998). I. Formation and rise of a bubble stream in a viscous liquid. *European Physical Journal B, 4*(3), 369–377. https://doi.org/10.1007/s100510050392.

Sun, L.i., Bi, X.-K., Lin, H., Zhao, J.-W., & Cai, J.-R. (2013). On-line detection of eggshell crack based on acoustic resonance analysis. *Journal of Food Engineering, 116*(1), 240–245. https://doi.org/10.1016/j.jfoodeng.2012.11.001.

Tunick, M. H., Onwulata, C. I., Thomas, A. E., Phillips, J. G., Mukhopadhyay, S., Sheen, S., Liu, C.-K., Latona, N., Pimentel, M. R., & Cooke, P. H. (2013). Critical Evaluation of Crispy and Crunchy Textures: A Review. *International Journal of Food Properties, 16*(5), 949–963. https://doi.org/10.1080/10942912.2011.573116.

van Ruth, S., Dekker, P., Brouwer, E., Rozijn, M., Erasmus, S., & Fitzpatrick, D. (2019a). The sound of salts by Broadband Acoustic Resonance Dissolution Spectroscopy. *Food Research International, 116*, 1047–1058. https://doi.org/10.1016/j.foodres.2018.09.044.

van Ruth, S. M., Hettinga, F., Dekker, P., & Fitzpatrick, D. (2019b). The sound of the sand from the Dutch shores. *Applied Acoustics, 154*, 1–10. https://doi.org/10.1016/j.apacoust.2019.04.026.

Vargaftik, N. B., Volkov, B. N., & Voljak, L. D. (1983). International Tables of the Surface Tension of Water. *Journal of Physical and Chemical Reference Data, 12*(3), 817–820. https://doi.org/10.1063/1.555688.

Vos, B., Crowley, S. V., O'Sullivan, J., Evans-Hurson, R., McSweeney, S., Krüse, J., Rizwan Ahmed, M., Fitzpatrick, D., & O'Mahony, J. A. (2016). New insights into the mechanism of rehydration of milk protein concentrate powders determined by Broadband Acoustic Resonance Dissolution Spectroscopy (BARDS). *Food Hydrocolloids, 61*, 933–945. https://doi.org/10.1016/j.foodhyd.2016.04.031.

Wold, S., Sjöström, M., & Eriksson, L. (2001). PLS-regression: A basic tool of chemometrics. *Chemometrics and Intelligent Laboratory Systems, 58*(2), 109–130. https://doi.org/10.1016/S0169-7439(01)00155-1.

Wu, S., Fitzpatrick, J., Cronin, K., Ahmed, M. R., Fitzpatrick, D., & Miao, S. (2019). Application of broadband acoustic resonance dissolution spectroscopy (BARDS) to the gas release behaviour during rehydration of milk protein isolate agglomerates. *Journal of Food Engineering, 253*, 14–20. https://doi.org/10.1016/j.jfoodeng.2019.02.010.

Zahedi, P., Saleh, R., Moreno-Atanasio, R., & Yousefi, K. (2014). Influence of fluid properties on bubble formation, detachment, rising and collapse; Investigation using volume of fluid method. *Korean Journal of Chemical Engineering, 31*(8), 1349–1361. https://doi.org/10.1007/s11814-014-0063-x.

Zhang, H. L., & Han, S. J. (1996). Viscosity and density of water+sodium chloride+potassium chloride solutions at 298.15 K. *Journal of Chemical and Engineering Data, 41*(3), 516–520. https://doi.org/10.1021/je9501402.